J. Chem. Lett. 4 (2023) 200-210

Research Article

Journal of Chemistry Letters
journal homepage: www.jchemlett.com
ISSN (online) 2717-1892 (print) 2821-0123

Investigation of Electronic and Spectroscopic Properties of Phosphosilicate Glass Molecule (BioGlass 45S5) and Ti-BioGlass 45S5 by Quantum Programming

Mehmet Hanifi Kebiroğlu[1], Rebaz Obaid Kareem[2*], Othman Abdulrahman Hamad[3]

[1]*Department of Opticianry, Darende Bekir Ilicak Vocational School, Malatya Turgut Ozal University, Malatya, Türkiye*
[2]*Physics Department, College of Science, University of Halabja, 46018, Halabja, Iraq*
[3]*University of Raparin, College of Science, Department of Chemistry, 46012, Sulamani, Iraq*

ARTICLE INFO

Article history:
Received 16 September 2023
Received in revised form 1 January 2024
Accepted 1 January 2024
Available online 1 January 2024

Keywords:
Phosphosilicate,
HOMO-LUMO,
DOS,
FMO,
FTIR,
UV-spectroscopy,
NMR

ABSTRACT

In this study, when a Ti atom is added to Phosphosilicate (BioGlass 45S5), its characterization is investigated using quantum chemical calculations. The STO-3G base-set HF approach was used to ensure that the ground-state molecular shape of both Phosphosilicate and titanium Phosphosilicate (Ti- Phosphosilicate) was optimized. Many other quantum chemical properties were determined, such as the energy gap (E_{HOMO}-E_{LUMO}), electronic properties, global reactivity, molecule electrostatic potential (MEP) on surfaces, and nuclear magnetic resonance (NMR), FT-IR were calculated at the B3LYP/STO-3G theory level. NMR shows eight peaks of the chemical shift values of the (H, O, P, and Si) molecule both Phosphosilicate and Ti-Phosphosilicate. Some examples of thermodynamic quantities include entropy (S), molar heat capacity (Cv), and thermal energy (E). According to MEP the negative-charged electrophilic reactivity region of the molecule is orange-red. Blue represents the positively charged nucleophilic reactive zone. The HOMO and LUMO energy gaps were smaller in Ti-Phosphosilicate, indicating that the molecule under study had major chemical reactivity, biological activity, and polarizing ability.

1. Introduction

Bioglass is modified in several ways to boost its bioactivity all over the globe [1, 2]. There are two primary approaches to the production of bioglass. First, developed by Hench, is characterized by a low characteristic surface area, a smooth texture, and a dense composition [3, 4]. Higher gated ness and a noticeably greater specific surface area in the mesoporous region are characteristics of bioglasses generated from sol-gel. because of their biological compatibility, resistance to corrosion, and mechanical qualities, pure titanium (Ti) and its alloyed forms, such as stainless steel, are still regarded as the best materials for the production of orthopaedic and dental implants [5, 6]. There have been many different suggestions made for surface alterations to investigate the osseointegration effectiveness of titanium implants [7]. The majority of dental implants have a rough body that is obtained by the use of procedures such as sandblasting, grinding with coarse grit, and acid etching (SLA) [8, 9]. During the coating of the titanium surface with a variety of bioactive materials and the subsequent creation of bioglass layers, the surface morphology of the Ti was encouraged to boost its biocompatibility as well as the effects of the osteoinductive proteins [10, 11]. Ti is often doped with ceramics biomaterial such as hydroxyapatite (HAp) to preserve its carbon-based ability to connect to bone and teeth, and it also forms hard bioactive materials that may serve as bone replacements [12, 13]. The chemical compositions of Phosphosilicate and Ti-Phosphosilicate are shown in **Fig**.

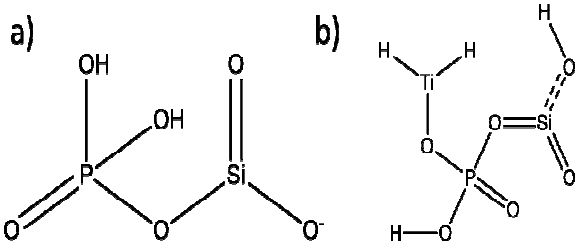

Fig. 1. Skeletal formula a) Phosphosilicate b) Ti-Phosphosilicate

∗ Corresponding author. Tel. +0647701054165; e-mail: rebaz.kareem@uoh.edu.iq
https://doi.org/ 10.22034/jchemlett.2024.416584.1138

The mechanical characteristics of alloys based on Ti are very important. However, it has relatively poor osseointegration capabilities even though it is normally well tolerated in physiological environments. To optimize the osseointegration of these materials, two different solutions are applied: The first method is surface modification, which is a more complicated method, and the manufacture of composite materials is the second aspect of the industry [14, 15]. Throughout the process of surface modification, the top layer of the titanium is altered using a variety of chemical and electrochemical processes that render it bioactive. Alternatively, bioactive doping may be placed using a technology such as electrophoresis and deposition technique (EPD), which is another option [16, 17]. The second strategy that I propose involves mixing the main material with bioactive components of ceramic biomaterials such as hydroxyapatite or bioglass to produce composites [18, 19]. The microstructure of the compound, the volume ratios of the various phases, and the kind of interaction that exists between the components all have a significant role in determining the physical characteristics of the composite. Additionally, it has been shown that the osseointegration capability of bioglass 45S5 composites is superior to that of pure titanium, particularly in the post-implantation phases [20, 21].

2. Calculation Methods

Density functional theory (DFT) and HF techniques are excellent for chemical compound stability and reactivity analysis. or more than two electrons. which consists mostly of contributions from promotions. Creating theoretical chemical models that accurately reflect this variety at a cost, and price is hard. Hartree-Fock (HF) is widely used now, however, it has major limitations [22]. With the assistance of Hartree-Fock's self-congruent field theory, we can carry out these computations [23]. The average spherical potential of an atom's electron is calculated by solving the Schrödinger equation. HOMO, and LUMO energy measurements and chemical reaction descriptions for systems of molecules are used to characterize a chain of reactions and determine the system's most reactive places [24]. Molecular reactivity and conductivity depend on HOMO and LUMO levels, which are affected by the energy bandgap or (HOMO-LUMO) molecular orbitals [25]. The polarizability of individual molecules is a factor that determines both optical activity and biological activity (biological activity). Below is an illustration of the parameter formula that was utilized for this:

$$I = -E_{HOMO} \tag{1}$$

$$A = -E_{LUMO} \tag{2}$$

$$\eta = \frac{1}{2}\left[\frac{\partial^2 E}{\partial^2 N}\right]_{v(r)} = \frac{I - A}{2} \tag{3}$$

$$\langle \alpha \rangle = \frac{1}{3}\left[\alpha_{xx} + \alpha_{yy} + \alpha_{zz}\right]\sigma = \frac{1}{\eta} \tag{4}$$

$$\text{Pi} = -\chi = \left[\frac{\partial E}{\partial} N\right]_{V(r)} = -\left(\frac{I+A}{2}\right) \tag{5}$$

$$\mu = \frac{-(I+A)}{2} \tag{6}$$

$$\omega = \frac{\chi^2}{2\eta} \tag{7}$$

$$\varepsilon = \frac{1}{\omega} \tag{8}$$

$$\omega^{+} = \frac{(I+3A)^2}{16(I-A)} \tag{9}$$

$$\omega^{-} = \frac{(3I+A)^2}{16(I-A)} \tag{10}$$

Equation 10 may be ascribed to the density of states (DOS), which is the sum of the final states, which is highly significant in finding the ratios. DOS is essential for evaluating the transition rates. DOS is not a static operating system. In meaning that, the DOS is not a natural number, but it is something that may be influenced to improve the operation of the device. Measuring the states following a certain wavenumber allows one to determine the electronic or photonic DOS $V(D) = L^D$ value and expressions are written in such a way that each side of the box has the length L. For periodic boundary conditions, the smallest possible $\frac{2\pi}{L}$ component of the wave vector is achieved by multiplying the mod count by D to get the total mod count. The following is a function of DOS in terms of the wave number:

$$\rho(k) = \frac{1}{V(D)}\frac{dN(k)}{dk} = s\left(\frac{1}{(2\pi)^D}\right)\Omega_D k^{D-1} \tag{11}$$

This is the equation that describes angular integrals, $\Omega_1 = 2, \Omega_2 = 2\pi, \Omega_3 = 4\pi,$, where s denotes the spin or polarisation degrees of freedom for waves, and s = 2 denotes that both electrons and photons have this degree of freedom, DOS employs size-specific measures such as states per cubic meter per inverse meter. Using this connection, we may express DOS in terms of energy (e.g., states per cubic meter per joule).

$$\rho(E)\,dE = \rho(k)\,dk \tag{12}$$

Carriers in the conduction band or valence band have a 3-D density of states (DOS) that is, under the parabolic approximation for bandgap energy:

$$\rho_c(E) = \frac{\sqrt{2}m_c^{3/2}}{\pi^2\hbar^3}\sqrt{E - E_g} \; and \; \rho_v(E) = \frac{\sqrt{2}m_V^{3/2}}{\pi^2\hbar^3}\sqrt{-E} \tag{13}$$

Electronic DOS is used to express carrier density:

$$n + \Delta n = \int dE\,\rho_c(E)\,f\left(E, E_{Qc}\right) \tag{14}$$

$$\rho + \Delta n = \int dE\,\rho_v(E)\,f\left(E, E_{Qv}\right) \tag{15}$$

Because photons have a linear energy-momentum relationship, the 3-D photonic DOS in a material with (actual) dielectric permittivity is provided below for accuracy. The dielectric function is expressed by the true component of the refractive index rr, and the free space ε_0 permittivity.

$$\rho_{ph}(E) = \frac{n_r^3}{\pi^2\hbar c}\left(\frac{E}{\hbar c}\right)^2 \tag{16}$$

According to equation 15, the photonic density of states (DOS) is defined as the number of photon states in a single energy reduction per unit volume per unit energy, dE.

2.1 Modern Quantum Chemistry Program Package

The chemical community as a whole uses theoretical and algorithmic developments for calculating electronic structures. Some examples include the use of fast Hartree-Fock (HF) computation techniques, linear scaling examination of energy, nuclear magnetic resonance (NMR) chemical shifts and electrical characteristics, quick auxiliary principal function ways of associating energy and gradients, and the relationship of mass-excitation kinetic equations. Potential energy surfaces may be investigated using a variety of techniques. It finds use in a wide range of scientific fields, including theoretical chemistry, computational quantum chemistry, and molecular physics, as well as computer science, applied mathematics, and electronic structure theory. In theory, many of the basic features of chemistry, such as molecule structures, the relative energy of distinct structures, and spectroscopic investigations, may be expected directly from quantum mechanics. It was first acknowledged by pioneers like Dirac and Lewis, but it is hard to get directly, to mention only two. Other than the most basic model systems, like the hydrogen atom, there are no analytical solutions. As a result, a numerical method should be investigated [26, 27].

3. Result and Discussion

3.1 Geometry Optimization

For this investigation, the Gaussian 09W package program was used [28]. The Hartree-Fock (HF) techniques were used to do theoretical computations on the substances that were researched. One of the most commonly utilized exchange-correlation functionals in HF computations is the B3LYP mixed functional, based on Becke's [29], exchange functional with three parameters and the correlation functional developed by Lee, Yang, and Parr [30]. Through the use of the STO-3G basis set, we were able to optimize the form of the molecule, ascertain its geometric features, and ascertain its minimum molecular energy. To determine the Mulliken charges, and boundary orbitals, the B3LYP/STO-3G approach was used. At its most fundamental level, geometry optimization is a two-step procedure that predicts the 3-D spatial arrangement of atoms inside a molecule. This arrangement may be seen from any angle. The optimized structures of the substances under study are shown in **Figure 2**.

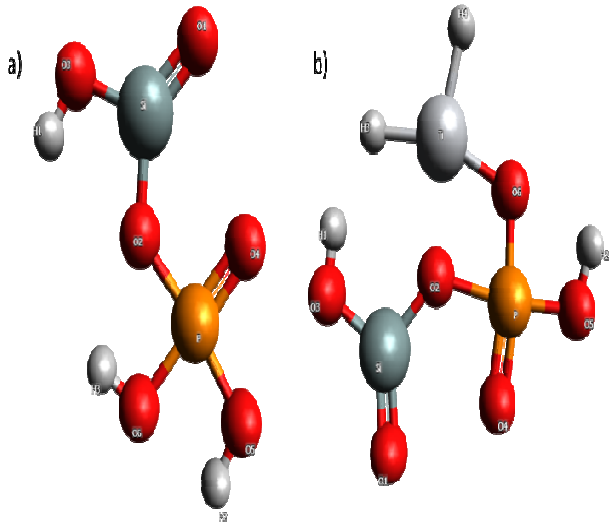

Fig. 2. Optimize the structure of a) Phosphosilicate b) Ti-Phosphosilicate

3.2 The thermochemical process

In this current study, the physical and thermodynamic parameters connected with this compound were calculated when the Ti atom was added to Phosphosilicate (BioGlass 45S5), using ground-state molecular geometry, and the Ti-bonded molecule of the Phosphosilicate was optimized using the STO-3G base-set HF method. The parameters of thermal entropy (S), energy (E), and molar heat capacity (Cv) are all examples of thermal properties. As indicated in **Table 1**, the values of E, S, and Cv vary when the solvent medium transitions from the gas phase to the solvent medium. These changes are influenced by the polarity of the solvent, and they also modify the molecular vibrations.

Table 1 Coefficients of thermodynamics Using a Ti component, Phosphosilicate glass (BioGlass 45S5)

Calculation of Parameters	unit	Phosphosilic	Ti - Phosphosilic
E (Thermal)	**kcal/mol**	45.168	
Cv	**cal/mol.K**	27.977	
S	**cal/mol.K**	89.320	

3.3 Frontier Molecular Orbital Analysis (FMO)

Accordance molecular orbital theory, the LUMO (Lowest Unoccupied Molecular Orbital), and HOMO (Highest Occupied Molecular Orbital) are the molecular orbitals with the most and least electrons, respectively. Because of their significance in chemical processes, HOMO and LUMO orbitals are sometimes called prime orbitals. Chemical stability has been defined as the difference between the HOMO and LUMO energy levels of a molecular structure [27]. In situations when the energy levels of the interaction orbitals of molecules are close to one another, the energy difference E is likewise lowered. This makes it easier for the reactants to interact with one another and perform a chemical reaction. Decrease the amount of energy HOMO-LUMO generates a large amount of molecular activity while simultaneously producing a small amount of chemical stability.

It is necessary to estimate both low and high electron density areas inside a molecule to have a better knowledge of numerous chemical processes. It is possible to use frontier molecular orbital analysis to make predictions about the electrophilic and nucleophilic regions of molecules to get a deeper comprehension of the chemical reactivity of organic species' chemical properties [31, 32]. In the FMO theory, the lowest empty orbital is located in an electrophilic zone because its electrons are extremely reactive and ready to take part in a reaction [33].

When there is a greater amount of HOMO energy, the HOMO electrons will be able to move around more freely. There is a greater amount of electron mobility, the compounds indicate a higher level of activity. The LUMO energy levels are determined by the electron acceptor density of the material. The lower the LUMO energy, the higher the activity level of the particle. Additionally, the energy gap of a molecule, denoted by the letter E, is equivalent to the difference in energy level between the LUMO and HOMO states of the molecule [34, 35]. This parameter is used in the calculation of the characteristic called reactivity. Increasing the softness value and decreasing the hardness value both contribute to an improvement in the activity of the molecules. Phosphosilicate's, and Ti-Phosphosilicate HOMO-LUMO energy level diagram and structure are shown in **Figure 3**:

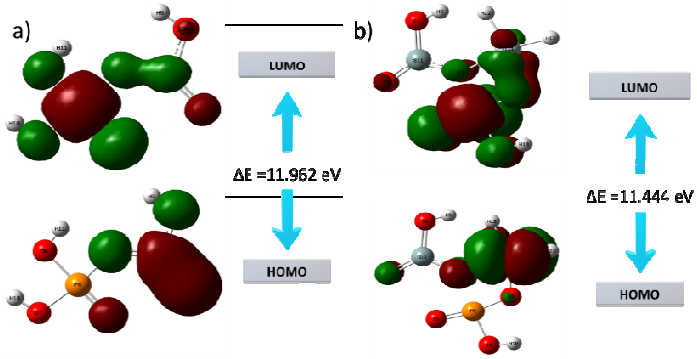

Fig. 3. HOMO-LUMO structure with the energy level diagram of a) Phosphosilicate and b) Ti-Phosphosilicate

Modeling molecular characteristics, optical activity, and biological function all benefit greatly from an accurate representation of the polarizability of each of the molecules. These equations are used to calculate ionization energy (I), electron affinity (A), chemical potential (Pi), electronegativity (χ), spherical hardness (η), softness (σ), **Dipole Moment (μ),** electrophilicity (ω), electron-accepting (ω^{+}), electron donating (ω^{-}), nucleophilicity (ε). The B3LYP/STO-3G ground state gas phase chemistry results are shown in **Table 1**. We may utilize the theoretical predictions made by quantum chemical parameters to learn about molecular activity.

The fact that the HOMO and LUMO energy gap had a smaller value Ti-Phosphosilicate, indicated that the molecule under research had high degrees of chemical reactivity, biological activity, and polarizing ability, in addition to having a lower level of stability. Phosphosilicate soft molecules (0.16 eV^{-1}) are more

reactive than Ti-Phosphosilicate (0.17 eV^{-1}) hard ones because they donate electrons quickly. More molecule hardness means less softness, which means that the energy band gap is proportional to molecule hardness [36-38]. Chemical characteristics that are closely related and may be changed by one another include electronegativity and electrical potential. The tendency of electrons to escape from an unstable system is symbolized by the chemical potential (μ). A complex is considered stable if its negative chemical potential means it does not spontaneously break down into its components as shown in **Figure 1**. An increased electronegativity value is because a more positively charged nucleus absorbs electrons more strongly. This research found that compared to pure Phosphosilicate (1.84 eV), Ti-Phosphosilicate (1.25 eV) has a stronger ability to absorb electrons due to its higher positively charged nucleus. One way to assess the energy reduction induced by the maximal electron flow between the giver and receiver is by using the HOMO-LUMO energy values to produce the global electrophilicity index (ω) [37]. Increasing the ionization energy, electron affinity, and softness of a material, as well as lowering the energy E_{HOMO}-E_{LUMO}, are all potential factors that might lead to an increase in chemical reactivity and a reduction in chemical stability at the same time.

Table 1. The calculated quantum chemical descriptors of a) Phosphosilicate b) Ti-Phosphosilicate

Compound	Phosphosilicate	Ti-Phosphosilicate
E_{HOMO} **(eV)**	-7.23	-7.56
E_{LUMO} **(eV)**	4.73	3.87
Δ*E* (eV)	11.96	11.44
η (eV)	5.98	5.77
σ (eV^{-1})	0.16	0.17
χ (eV)	1.25	1.84
Pi (eV^{-1})	-1.25	-1.84
ω (eV)	0.130	0.293
ε (eV)	7.69	7.51
$ω^+$(eV)	2.39	0.089
$ω^-$(eV)	1.50	0.102
μ (Depye)	-1.25	-1.84

3.4 Fourier Transform Infrared (FTIR) Spectroscopy

By absorbing incoming infrared light, infrared becomes active when the dipole moment of the compound shifts during vibration [39]. As an immediate result of this, symmetrical oscillations are rarely detected in the infrared spectrum. In the infrared spectrum, only some of the vibrations associated with a molecule's symmetry will be active if the molecule has a center of symmetry [40]. On the opposing side, asymmetric vibrations in every molecule could be seen. This lack of selectivity makes it possible to characterize almost all chemical groups, most especially amino acids and molecules of water, in a single sample, which is difficult to do using traditional spectroscopic methods [41]. One of the most effective approaches for characterizing a membrane's functional group and potential molecular interactions between chemical substances is Fourier transform infrared (FT-IR) spectroscopy [41, 42].

It is possible to identify several types of chemical compounds (such as aromatics) that cannot be seen in X-ray photoelectron spectroscopy spectra by learning the locations of IR absorption bands in the spectrum as wavenumbers. Generally speaking, IR spectroscopy may be utilized for both qualitative and quantitative studies across a broad range of materials and settings [43].

It displays the predicted FT-IR spectra (4500 cm-1 to 0 cm-1) of the investigated compounds, complete with absorption peaks. Harmonic frequencies are shown in the diagram. The harmonic frequencies are determined by multiplying the harmonic frequencies by the relevant measurement factor for every level of computation. The similarity in complexes implied similarity in the frequency of vibration and spectra. The vibrational frequency of a bond rises as the bond strength increases and the mass of the bond atom decreases, with the fundamentals of vibrational spectroscopy. In **Figure 4**, the peak number of 18 indicates the highest intensity, and the frequency indicates 504 cm^{-1}. Other permeability numbers—83, 79, 60, 74, 57, and 76 peak numbers—have been changed at a low level. It shows the energy range between 1386 cm^{-1} and 4275 cm^{-1} between 67 and 19 peak numbers.

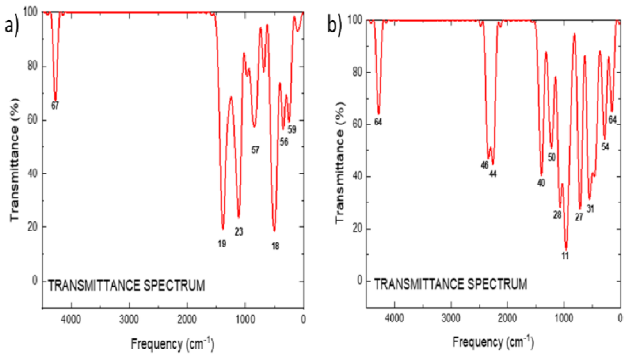

Fig. 4. FT-IR spectrum a) Phosphosilicate b) Ti-Phosphosilicate

Therefore, it is essential to determine the locations and sizes of all absorptions or peaks, vibrational types, and spectral pattern alterations while analyzing an FT-IR spectrum [44, 45].

3.5 Nuclear Magnetic Resonance Spectroscopy

One of the most useful spectroscopic methods for elucidating molecular structure is an analysis of nuclear magnetic resonance spectra (NMR). Whenever a paramagnetic material is present in an NMR spectroscopic study, two major appear. The first of these is known as line widening, while the second is contact shift. The significant change in chemical shift values experienced by atoms near a paramagnetic center is called contact shift. Line widening refers to a rise in half-height line widths as a result of fast relaxation owing to the interaction of the nuclear spin with the unpaired electron is called line broadening. Spectrum obtaining might be difficult in the presence of line widening. In this research study, Computational chemistry methods were used to determine chemical shifts of the substances examined at the B3LYP/STO-3G level. As a result, the carbon nuclei have less shielding. In regions that have less shielding, chemical shift values appear to be larger. Every Structure has opposing and adjacent positions. A rotational process replaces protons that are in opposing locations with one another. Because of this, we might consider them to be identical protons. The peaks of chemically equivalent protons are at the same chemical shift value. The values of the calculated chemical shift are shown in **Table 2**. The peaks in the complex spectra that stay constant or move to higher regions are a significant indication that describes both the complexation and the atoms involved in the coordination. Proton nuclei are heavily protected by their electrons and so peak at low ppm.

In **Figure 5** we can see that there are eight peaks. The chemical shift values of the 6-O proton are in the range of -585,252 ppm. Chemical shift values of 10-H-8-H protons range from 29.6385 ppm to 32.631 ppm. The chemical shift values of the 2-O proton are in the range of 77.4245 ppm. Chemical shift values of 7-O-3-O protons range from 264.3398 ppm to 267.7892 ppm. The chemical shift values of the 8-O proton are in the range of 308.6577 ppm. The chemical shift values of the 4-O proton are in the range of 365.1116 ppm. The chemical shift values of the 5-P proton are in the range of 389.1093 ppm. The chemical shift values of the 1-Si proton are in the range of 455.1318 ppm.

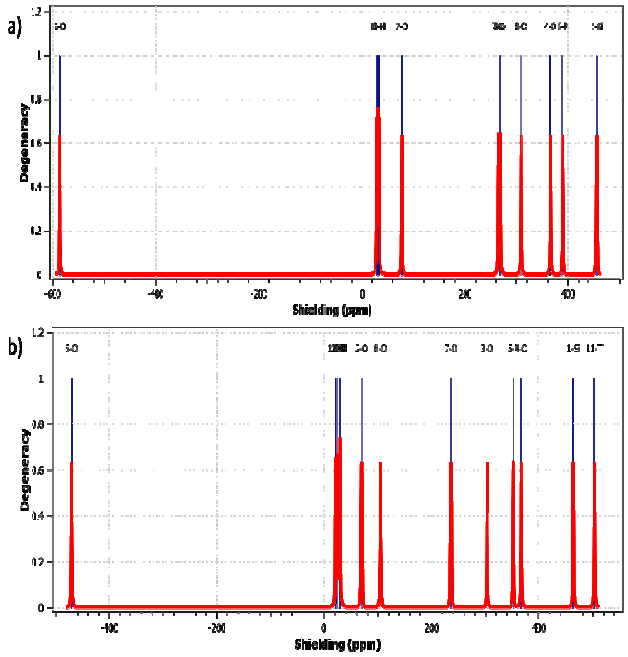

Fig. 5. NMR spectrum a) Phosphosilicate b) Ti-Phosphosilicate

Table 2. Chemical shifts a) Phosphosilicate b) Ti-Phosphosilicate

a) Method	Shielding (ppm)	b) Method	Shielding (ppm)
6-O	-585.252	6-O	-470.4582
10-H	29.6385	12-H	21.0313
11-H	31.1275	13-H	24.4527
9-H	32.631	10-H	27.9584
2-O	77.4245	9-H	29.1931
7-O	264.3398	2-O	69.2182
3-O	267.7892	8-O	104.9718
8-O	308.6577	7-O	236.4401
4-O	365.1116	3-O	303.3448
5-P	389.1093	5-P	351.7081
1-Si	455.1318	4-O	367.0151

3.6 UV–Visible Analysis

UV-visible spectroscopy was likely initially used by chemists, who made the subsequent discovery of molecular structure. The ability to investigate both the optical and electrical characteristics of nanoscale particles has been improved by optical-based techniques. **Figure 6a** shows the absorbance spectra and peak of the Phosphosilicate structure for B3LYP/STO-3G. The color of the structure may be seen in the 176 nm peak due to the visible and localized absorption there. The energy of the 176 nm peak is 11,962 eV. **Figure 6b** shows the absorbance

spectra and peak of the Ti-doped Phosphosilicate structure for B3LYP/STO-3G. The color of the structure may be seen in the 176 nm peak due to the visible and localized absorption there. The energy of the 682 nm peak is 11,444 eV.

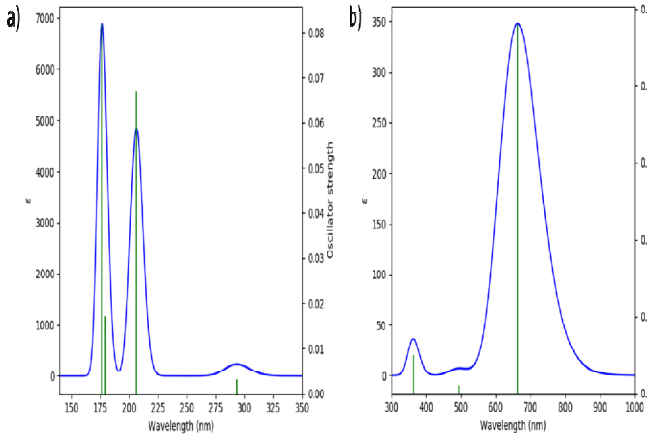

Fig. 6. UV-visible absorption spectrum a) Phosphosilicate b) Ti-doped Phosphosilicate

3.7 Density of States (DOS)

The density of states (Dos) is a term that refers to the ratio of the number of electronic states (orbitals) in an atom to the energy level of the atom. The DOS is an expression for the density of energy levels in a quantum mechanical structure, which may be thought of as the degree to which the electrons are "packed" in that system. Using Fermi energy (as determined by Fermi-Dirac statistics) and temperature, it represents the distribution of electrons in atomic orbitals i.e., or the occupancy of atomic orbitals by electrons. When the density of states is large, it means that there are lots of possible occupations for the electron state [45-47]. The density of states (DOS) as a function of energy may be determined with the use of the following formula:

$$DOS(E) = \sum g(E - \varepsilon_i) \qquad (17)$$

The energy levels of the modeled system, denoted by ε_i are a product of the electronic orbitals included, and the variables E and ε_i are used to calculate the function g [46, 48]. The DOS calculation in **Figure 7** depicts the HOMO-LUMO energy range of the pure Phosphosilicate and Ti-Phosphosilicate molecule. Doping a Ti compound with Phosphosilicate is investigated in this study via the lens of the density of states, which is utilized to determine how the occupancy of electrons is altered as a result of doping.

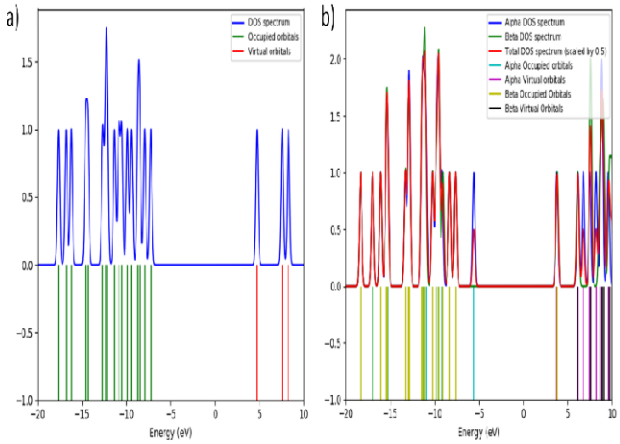

Fig. 7. The density of states (DOS) with the contribution a) Phosphosilicate b) Ti-Phosphosilicate

The effectiveness of the Ti compound has been shown in the change of bandgap energy as illustrated in **Table 1**. The molecules were doped with Ti compound, and the band gap energy decreased from 11.96 eV to 11.44 eV, while at the same time, electronegativity and softness increased from 1.25 to 1.84 eV, and 0.160 to 0.170 eV. This result indicates that bandgap energy responded by increasing gradually according to the electronegativity of the doping. In conclusion, the higher Phosphosilicate interaction energy indicates that the interacting system is thermodynamically preferable. We can conclude that, If an element has a greater electronegativity, then the bandgap will shift towards a lower energy level.

3.8 Molecular Electrostatic Potential (MEP)

Electrostatic potential maps (EPM) of the structure are a sort of analysis that is connected to the electronegativity and partial charges that exist on certain components. The Molecular Electrostatic Potential, often known as (MEP), is the energy that is associated with the relationship between the positive charge per unit and the overall distribution of charges in a system of molecules. Understanding bonding qualities with biological molecules, such as charge-dipole, dipole-dipole, and quadrupole-dipole interactions, may be accomplished with the use of MEP surface analysis, which is a beneficial tool [49]. The MEP map illustrates the areas of the molecule that are electron acceptors, electron donors, and neutral. With the use of the MEP map, it is possible to determine whether parts of the molecule have reactive areas that are electrophilic or nucleophilic. The surface map is shown with colors ranging from red to blue, with red representing the area with the highest concentration of electrons and blue representing the region with the lowest concentration as shown in **Figure 8.** The electron density was found to be lower in areas around the remainder of the molecule (green). The presence of

green coloration indicates that the hydrogen is in the electrophilic zone. Since the electrophilic potential of the Ti compound was found to rise from 0.130 to 0.293, the red zone decreased Figure 7 illustrates it. The ability of a molecule to interact with other molecules in chemical processes may be related to its electrophilic and nucleophilic areas. According to the results of this study, the molecule is more likely to display nucleophilic than electrophilic characteristics. On the MEP map, red indicates the area with the greatest negative potential (where the electron density is greater than the nucleus over the whole molecule), whereas blue indicates the area with the greatest positive potential (where partial positive charges dominate) [50]. Some factors that may affect the Potential Energy Map include higher levels of electron affinity, electronegativity, and dipole moment [38]. Each MEP is essential for intermolecular interaction when a pair of molecules are close together. The greatest negative MEP values indicate the most electrophilic areas of a molecule [51].

Lastly, the portions that are orange-red in color reflect the electrophilic reactivity section of the molecule, which has a negative charge. The positively charged region, also known as the nucleophilic reactive zone, is shown by the blue area. Red EP (strong-EP) > orange EP > yellow EP > green EP > blue EP (strong +EP) [52].

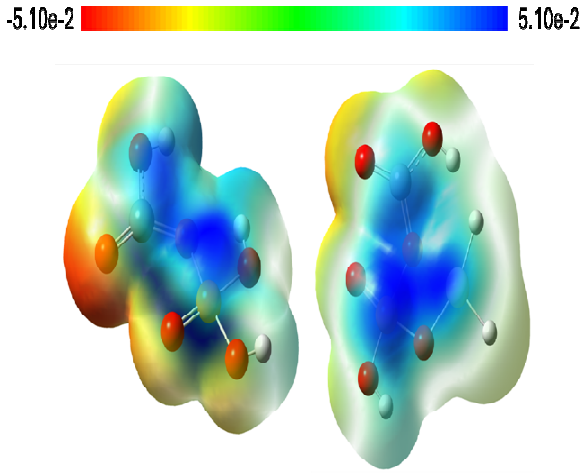

Fig. 8. Molecular Electrostatic Potential a) Phosphosilicate b) Ti-Phosphosilicate

4 Conclusion

For the Phosphosilicate and Ti- Phosphosilicate molecules, quantum computational and spectroscopic vibrational analyses were performed to interpret the chemical and physical properties of the molecule. The HOMO energy was mostly observed in the Si atom. In LUMO, it was observed mostly in P atoms. For the HOMO-LUMO energy gaps, E_{HOMO} = -7.231 eV and E_{LUMO} = 4.731 eV, ΔE = 11,962 eV, suggesting that charge transfer has taken place. FT-IR spectroscopy shows estimated FT-IR spectra in the range of 4500 cm^{-1} to 0 cm^{-1} showing absorption peaks. The peak number of 18 indicates the highest intensity, and the frequency indicates 504 cm^{-1}. The NMR spectra revealed eight distinct peaks. The chemical shift values of the 6-O proton are in the range of -585,252 ppm. Chemical shift values of 10-H-8-H protons range from 29.6385 ppm to 32.631 ppm. The chemical shift values of the 2-O proton are in the range of 77.4245 ppm. Chemical shift values of 7-O-3-O protons range from 264.3398 ppm to 267.7892 ppm. The chemical shift values of the 8-O proton are in the range of 308.6577 ppm. The chemical shift values of the 4-O proton are in the range of 365.1116 ppm. The chemical shift values of the 5-P proton are in the range of 389.1093 ppm. Chemical shift values of the 1-Si proton were seen in the range of 455.1318 ppm. Using UV-visible spectroscopy, the absorbance spectra and peak of the Phosphosilicate structure are observed. The 176 nm peak indicates the color of the structure because this absorption is visible and occurs in this region. According to MEP the negative-charged electrophilic reactivity region of the molecule is orange-red. Blue represents the positively charged nucleophilic reactive zone. It is thought that with the development of Bioglass, new techniques will be developed in optical studies.

Finally, The fact that the HOMO and LUMO energy gap had a smaller value Ti-Phosphosilicate, indicated that the molecule under research had high degrees of chemical reactivity, biological activity, and polarizing ability, in addition to having a lower level of stability. Phosphosilicate soft molecules (0.16 eV^{-1}) are more reactive than Ti-Phosphosilicate (0.17 eV^{-1}) hard ones because they donate electrons quicker.

References

[1] R. G, Furlan, W.R, Correr, A.F.C, Russi, M.R, da Costa Iemma., E. Trovatti. and E. Pecoraro, 2018. Preparation and characterization of boron-based bioglass by sol– gel process. *Journal of Sol-Gel Science and Technology*, *88*(2018).181-191.

[2] M. Schumacher, P. Habibovic. and S. Van Rijt., 2021. Mesoporous bioactive glass composition effects on degradation and bioactivity. *Bioactive Materials*, *6*(7), (2021).1921-1931.

[3] L. Hench. L. The story of Bioglass®, 17 (11), (2006): 967-978.

[4] T.H. Dang., T.H. Bui., E.V. Guseva, Ta, A.T., Nguyen, A.T., T.T.H. Hoang. and X.V. Bui. Characterization of bioactive glass synthesized by sol-gel process in hot water. *Crystals*, *10*(6), (2020).529.

[5] D.J. Cohen, A. Cheng., K. Sahingur., R.M. Clohessy, L.B. Hopkins, B.D. Boyan. and Z. Schwartz. Performance of laser sintered Ti–6Al–

4V implants with bone-inspired porosity and micro/nanoscale surface roughness in the rabbit femur. *Biomedical Materials*, *12*(2), (2017).025021.

[6] A.M. Khorasani, GM. oldberg., E.H. Doeven. and G. Littlefair., Titanium in biomedical applications—properties and fabrication: a review. *Journal of biomaterials and tissue engineering*, *5*(8), (2015).593-619..

[7] X.P. Tan., Y.J. Tan, C.S.L. Chow, S,B. Tor. and W.Y. Yeong,. Metallic powder-bed based 3D printing of cellular scaffolds for orthopaedic implants: A state-of-the-art review on manufacturing, topological design, mechanical properties and biocompatibility. *Materials Science and Engineering: C*, *76*, (2017).1328-1343.

[8] F. Trevisan, F. Calignano, A. Aversa., G. Marchese., M. Lombardi., S. Biamino, D. Ugues,. and D. Manfredi,. Additive manufacturing of titanium alloys in the biomedical field: processes, properties and applications. *Journal of applied biomaterials & functional materials*, *16*(2), (2018).57-67.

[9] Yabutsuka, T., Mizuno, H. and Takai, S., 2019. Fabrication of bioactive titanium and its alloys by combination of doubled sandblasting process and alkaline simulated body fluid treatment. *Journal of the Ceramic Society of Japan*, *127*(10), pp.669-677.

[10] N.K Awad., S.L. Edwards,. and Y.S. Morsi., A review of TiO2 NTs on Ti metal: Electrochemical synthesis, functionalization and potential use as bone implants. *Materials Science and Engineering: C*, *76*, (2017).1401-1412.

[11] G. Wang., M. Dargusch., and N. Doan, Material Perspectives of the Dental Implants: A Review. in *6th International Conference on the Development of Biomedical Engineering in Vietnam (BME6) 6*.(2018) Springer.

[12] C. Yan., L. Hao., A. Hussein., Q. Wei. and Y. Shi.,. Microstructural and surface modifications and hydroxyapatite coating of Ti-6Al-4V triply periodic minimal surface lattices fabricated by selective laser melting. *Materials Science and Engineering: C*, *75*, (2017).1515-1524..

[13] H.L. Oliveira., W.L. Da Rosa., C.E. Cuevas-Suárez., N.L. Carreño., A.F. da Silva, T.N. Guim., O.A. Dellagostin. and E. Piva., Histological evaluation of bone repair with hydroxyapatite: a systematic review. *Calcified tissue international*, *101*, (2017).341-354.

[14] j.j. Jasinski., M. Lubas, L. Kurpaska,, W. Napadlek,. and M. Sitarz.,. Functionalization of Ti99. 2 substrates surface by hybrid treatment investigated with spectroscopic methods. *Journal of Molecular Structure*, *1164*, (2018).412-419.

[15] M. Alksne., M. Kalvaityte., E. Simoliunas., I. Rinkunaite., I. Gendviliene., J. Locs., V. Rutkunas. and V. Bukelskiene., In vitro comparison of 3D printed polylactic acid/hydroxyapatite and polylactic acid/bioglass composite scaffolds: Insights into materials for bone regeneration. *Journal of the mechanical behavior of biomedical materials*, *104*, (2020).103641.

[16] H.H. Rodríguez., A. Maldonado-Reyes,. and D.A. Cortés-Hernández., Electrophoretic deposition of a bioactive Si, Ca-rich glass coating on 316L stainless steel for biomedical applications. *Journal of applied research and technology*, *9*(3), (2011).314-323.

[17] S. Erakovic., A. Jankovic., G.C. Tsui., C.Y. Tang., V. Miskovic-Stankovic,. and T. Stevanovic., Novel bioactive antimicrobial lignin containing coatings on titanium obtained by electrophoretic deposition. *International journal of molecular sciences*, *15*(7), (2014).12294-12322.

[18] D. Hanaor., M. Michelazzi., P. Veronesi.,C. Leonelli., M. Romagnoli. and C. Sorrell.,. Anodic aqueous electrophoretic deposition of titanium dioxide using carboxylic acids as dispersing agents. *Journal of the European Ceramic Society*, *31*(6), (2011).1041-1047.

[19] M.Q. Li., L.J . Qu., Li, B., Zhuang, M.H. and S.Q. Yang., May. Ti-Glass Biocomposite Coating Materials and their Crystallization Dynamics. In *Materials Science Forum* (Vol. 610, (2009). 1211-1214). Trans Tech Publications Ltd.

[20] K. Niespodziana., K. Jurczyk.,J. Jakubowicz. and M. Jurczyk.. Fabrication and properties of titanium–hydroxyapatite nanocomposites. *Materials Chemistry and Physics*, *123*(1), (2010).160-165.

[21] M. Kaczmarek., M.U. Jurczyk., B.Rubis., A. Banaszak., A. Kolecka., A. Paszel., K. Jurczyk., M. Murias., J. Sikora. and M. Jurczyk.,. In vitro biocompatibility of Ti□45S5 bioglass nanocomposites and their scaffolds. *Journal of Biomedical Materials Research Part A: An Official Journal of The Society for Biomaterials, The Japanese Society for Biomaterials, and The Australian Society for Biomaterials and the Korean Society for Biomaterials*, *102*(5), (2014).1316-1324.

[22] V. Fock.,. Näherungsmethode zur Lösung des quantenmechanischen Mehrkörperproblems. *Zeitschrift für Physik*, *61*, (1930).126-148.

[23] H. Haken. and H.C. Wolf.,. *Atomic and quantum physics: an introduction to the fundamentals of experiment and theory*. Springer Science & Business Media(2012).

[24] E. Pidcock., H.V. Obias., C.X. Zhang., K.D. Karlin. and E.I. Solomon.,. Investigation of the reactive oxygen intermediate in an arene

hydroxylation reaction performed by xylyl-bridged binuclear copper complexes. *Journal of the American Chemical Society*, *120*(31), (1998).7841-7847.

[25] E.I. Solomon., P. Chen., M. Metz., S.K. Lee,. and A.E. Palmer.,. Oxygen binding, activation, and reduction to water by copper proteins. *Angewandte Chemie International Edition*, *40*(24), (2001).4570-4590.

[26] S. Acharya., D. Bhattacharjee., J. Sarkar. and G.B. Talapatra., 2004. Spectroscopic study of non-amphiphilic 2-(4-biphenylyl)-5-(4-tert-butylphenyl)-l, 3, 4-oxadiazole aggregates at air–water interface and in Langmuir–Blodgett films. *Chemical physics letters*, *393*(1-3), (2004).1-6.

[27] P. Tecmer,. and K. Boguslawski.. Geminal-based electronic structure methods in quantum chemistry. Toward a geminal model chemistry. *Physical Chemistry Chemical Physics*, *24*(38), (2022).23026-23048.

[28] M.J Frisch, G.W. Trucks., H.B. Schlegel., G.E. Scuseria., M.A. Robb., J.R. Cheeseman., G. Scalmani., V. Barone., B. Mennucci., G.A. Petersson. and H. Nakatsuji., Uranyl Extraction by N, N-Dialkylamide Ligands Studied by Static and Dynamic DFT Simulations. In *Gaussian 09*.(2009) Gaussian Inc Wallingford.

[29] A.D Becke.. Density-functional exchange-energy approximation with correct asymptotic behavior. *Physical review A*, *38*(6), (1988).3098.

[30] A.D. Becke.,. A new mixing of Hartree–Fock and local density□functional theories. *The Journal of chemical physics*, *98*(2), (1993).1372-1377.

[31] L. Salem.,. The molecular orbital theory of conjugated systems. (1966),*(No Title)*..

[32] M. Karplus,. and R.N. Porter.,. Atoms and molecules; an introduction for students of physical chemistry. *Atoms and molecules; an introduction for students of physical chemistry. (1970)*.

[33] P.W. Ayers,. and R.G. Parr.. Variational principles for describing chemical reactions: the Fukui function and chemical hardness revisited. *Journal of the American Chemical Society*, *122*(9), (2000).2010-2018.

[34] E. Knözinger., 1986. PR Griffiths, JA de Haseth: Fourier Transform Infrared Spectroscopy, Vol. 83 aus der Reihe: Chemical Analysis—A Series of Monographs of Analytical Chemistry and Its Applications, John Wiley+ Sons, Chichester, New York, Brisbane, Toronto, Singapore 1986. 656 Seiten, Preis:£ 76.75.

[35] R.O. Kareem., M.H. Kebiroğlu., O.A. Hamad., O. Kaygili. and N. Bulut,. Epinephrine Compound: Unveiling Its Optical and Thermochemical Properties via Quantum Computation Methods. 6(4).(2024).415-427.

[36] V.D. Singh,., A.U. Kamni., Y. Khajuria., B. Narayana., R. Srinivasan., B.K. Sarojini., S. Anthal. and R. Kant.,. Synthesis, FT-IR, UV-VIS, DFT studies and SCXRD structure of 1-(tert-butyl) 3-ethyl-3-(hydroxy (thiophen-2-yl) methyl) piperidine-1, 3-dicarboxylate. *Indian Journal of Chemistry-Section B (IJC-B)*, *59*(7), (2020).1043-1056.

[37] Mumit, M.A., Pal, T.K., Alam, M.A., Islam, M.A.A.A.A., Paul, S. and Sheikh, M.C.,. DFT studies on vibrational and electronic spectra, HOMO–LUMO, MEP, HOMA, NBO and molecular docking analysis of benzyl-3-N-(2, 4, 5-trimethoxyphenylmethylene) hydrazinecarbodithioate. *Journal of molecular structure*, *1220.(2020).* 128715,

[38] O. Hamad,. R.O. Kareem,. And O. Kaygili., 2023. Density Function Theory Study Of The Physicochemical Characteristics Of 2-Nitrophenol. *Journal Of Physical Chemistry And Functional Materials*, *6*(1), 2023.70-76.

[39] R.G. Parr,. and W. Yang.,. Density functional approach to the frontier-electron theory of chemical reactivity. *Journal of the American Chemical Society*, *106*(14), (1984).4049-4050.

[40] L. Qiu., K. Levine., K.S. Gajiwala., C.N. Cronin., A. Nagata., E. Johnson., M. Kraus., J. Tatlock., R. Kania., T. Foley. and S. Sun.,. Small molecule inhibitors reveal PTK6 kinase is not an oncogenic driver in breast cancers. *PLoS One*, *13*(6), (2018).e0198374.

[41] Messick, T.E., Russell, N.S., Iwata, A.J., Sarachan, K.L., Shiekhattar, R., Shanks, J.R., Reyes-Turcu, F.E., Wilkinson, K.D. and Marmorstein, R.,. Structural basis for ubiquitin recognition by the Otu1 ovarian tumor domain protein. *Journal of Biological Chemistry*, *283*(16), (2008).11038-11049.

[42] M.A. Mohamed., WNW. Salleh., J. Jaafar., Z.A.M. Hir., M.S. Rosmi., M.A. Mutalib., A.F. Ismail. and M. Tanemura.,. Regenerated cellulose membrane as bio-template for in-situ growth of visible-light driven C-modified mesoporous titania. *Carbohydrate polymers*, *146*, (2016).166-173.

[43] D.L. Pavia., G.M. Lampman., G.S. Kriz. and J.A. Vyvyan.,. *Introduction to spectroscopy*. Cengage learning. 2014.

[44] B.C. Smith.,. *Fundamentals of Fourier transform infrared spectroscopy*. CRC press. 2011.

[45] Z.M. Khoshhesab.,. Reflectance IR spectroscopy. *Infrared spectroscopy-Materials science, engineering and technology*, *11*, (2012).233-244.

[46] F. İsen., O. Kaygili., N. Bulut., T. Ates., F. Osmanlıoğlu., S. Keser., B. Tatar., I. Özcan., B.

Ates., F. Ercan. I.Ercan, and R.O. Kareem.,. Experimental and theoretical characterization of Dy-doped hydroxyapatites. *Journal of the Australian Ceramic Society*, (2023).1-16.

[47] R.O. Kareem., O. Kaygili., T. Ates., N. Bulut., S. Koytepe., A. Kuruçay., F. Ercan,. and I. Ercan.,. Experimental and theoretical characterization of Bi-based hydroxyapatites doped with Ce. *Ceramics International*, *48*(22), (2022).33440-33454.

[48] A.A. Korkmaz.,L.O. Ahmed., R.O. Kareem., H. Kebiroglu., T. Ates,. N. Bulut., O. Kaygili. and B. Ates.,. Theoretical and experimental characterization of Sn-based hydroxyapatites doped with Bi. *Journal of the Australian Ceramic Society*, *58*(3), (2022).803-815.

[49] C.J Cramer.,. Computational Chemistry, Theories and Models. 2004.

[50] I.N. Levine., D.H. Busch,. and H. Shull., . *Quantum chemistry* . Upper Saddle River, NJ: Pearson Prentice Hall.9. (2009).

[51] J.R. Hook,. and H.E. Hall., . *Solid state physics*, John Wiley & Sons, 2013.

[52] M. El Idrissi., S. Elharfaoui., Z. Zmirli., A. Mouhssine.,A. Dani., B. Salle., A. Tounsi., K. Digua. and H. Chaair.,. Theoretical and Experimental Study of the Orientation to the Most Effective Coagulant for Removing Reactive Black-5 Dye from Industrial Effluents. *Physical Chemistry Research*, *12*(1), (2024).229-248.